JOURNAL OF MATERIALS SCIENCE 32 (1997) 2637–2646

The structure and mechanical properties of thick cobalt electrodeposits

J. DILLE, J. CHARLIER, R. WINAND*
*Métallurgie Physique, CP 194/3 and *Métallurgie Electrochimie, CP 165,*
Université Libre de Bruxelles, Avenue F.D. Roosevelt, 50-B 1050 Bruxelles, Belgium

Cobalt electrodeposits have been produced in chloride solutions. Depending on the electrolysis parameters applied, two different structures for the electrodeposits, namely α and β cobalt were observed. Their characterization included hydrogen content measurement, the relative volume fraction of the α and β phases determined by X-ray diffraction, X-ray diffraction line profile analysis and microstructural investigation by optical microscopy, scanning electron microscopy and transmission electron microscopy. The influence of structure on mechanical properties was examined. The results showed that the ductility properties of the cobalt electrodeposits were highly sensitive to the structure. A higher β phase content that was measured in some deposits did not improve the ductility due to the existence of trapped hydrogen which always exists in such deposits. However, annealing treatments seem to be a promising route to optimize the ductility of cobalt electrodeposits.

1. Introduction

According to various authors [1–7], the structure of cobalt electrodeposits strongly depends on the composition of the electrolyte and on the electrolysis parameters such as the pH of the solution, the temperature and the current density. Three types of electrolyte are particularly utilized: sulphate solutions, chloride solutions or Watts type baths.

The principal structural feature of interest is the type of phases that occur in the deposits. Cobalt exists in two allotropic modifications, α and β. The α phase is hexagonal close-packed (HCP) and is thermodynamically stable up to 417 °C whereas the β phase is face-centered cubic (FCC) and is stable at temperatures higher than 417 °C. Although the electrolysis temperatures are well below 417 °C, the cobalt electrodeposits often simultaneously contain both phases. This is especially noticeable at low pH values and low deposition temperatures and is independant of the electrolyte used in the electrolysis. The presence of the face-centered cubic β phase at room temperature results from the small difference between the free energies of both modifications.

Another important structural feature of the electrodeposits is their fibrous texture. In this paper, the nature of the fibrous texture will be distinguished in terms of the crystallographic plane which is preferentially oriented parallel to the substrate. In cobalt electrodeposits, the hexagonal close-packed phase often exhibits an $\alpha\,(1\,1\,\bar{2}\,0)$ texture or an $\alpha\,(1\,0\,\bar{1}\,0)$ texture depending on the electrolysis conditions. If both phases are co-deposited, then a texture correspondence between HCP α and FCC β has been reported [4] to be:

$$\text{HCP}\,\alpha(1\,1\,\bar{2}\,0) + \text{FFC}\,\beta(2\,2\,0) \text{ or } \text{HCP}\,\alpha(1\,0\,\bar{1}\,0) + \text{FCC}\,\beta(4\,2\,2) \quad (1)$$

On the other hand, Sard *et al.* [1] have noted the occasional existence of a "pseudo random" structure in HCP cobalt deposits. In this context a "pseudo random" structure is one in which the basal planes $\alpha(0\,0\,0\,2)$ are almost never parallel to the substrate and no preferred orientation is shown for the other planes. Different structural features such as the surface appearance of deposits or the shape of grains are generally closely related to the texture.

Whilst there is a fairly detailed knowledge of the inter-relation between the electrolysis parameters and the structure of the electrodeposit very little work has been performed to relate the electrodeposit structure to observed properties of the electrodeposited cobalt. There are reports in the literature [8–10] on the influence of the electrodeposit structure on various magnetic properties. In addition, Feneau and Breckpot [3] have reported that cobalt electrodeposits with an HCP $\alpha(0\,0\,0\,2)$ texture – which is occasionally produced at high pH values in sulphate baths – are more brittle than deposits with a HCP $\alpha\,(1\,1\,\bar{2}\,0)$ or $\alpha\,(1\,0\,\bar{1}\,0)$ texture.

The purpose of the present work [11] is to study in more detail the relationships between the structure and mechanical properties of free standing cobalt electrodeposits. In particular we address the question as to if an increasing content of FCC β phase improves the ductility as has been established for cobalt strips

0022–2461

obtained by thermomechanical processes [12–14]. This behaviour could be explained by the fact that the limited number of slip systems in HCP metals restricts their ductility whereas the FCC metals with more slip systems generally exhibit a good ductility.

In order to reach this objective, different cobalt electrodeposits displaying the most frequently encountered structures are required. This can be achieved by investigating a wide range of pH. The deposits should be thick enough for their mechanical properties to essentially depend on the structure which is in turn controlled by the electrodeposition parameters. In this case, the role of the substrate influenced deposit zone can be minimized. The characterization of the deposits will aim at establishing accurate relations between the electrolysis parameters, the structure and observed properties.

2. Experimental procedure

2.1. Cobalt electrodeposition

In order to control the hydrodynamics during the cobalt deposition, a channel cell was used (see Fig. 1). The commercially pure copper cathode was polished using 600 grade abrasive paper and then the cathode was carefully cleaned with ethanol. The anode is a pure cobalt electrode. An additive free electrolyte containing 202 g dm^{-3} $CoCl_2 \cdot 6H_2O$ (0.85 M Co^{2+}) flowed parallel to the electrodes with a flow rate of 0.4 m s^{-1}.

The cobalt electrodeposits were obtained at a constant current density of 800 A m^{-2}. The temperature of the electrolyte was kept at 50 °C (25 °C for some deposits at pH 1.5 or at pH 4.0). The electrolyte pH values range from 1.0–5.0 and were adjusted by HCl additions.

During the electrolysis, the pH of the solution tends to increase. Some hydrochloric acid was added from time to time to adjust the pH with an accuracy of $\pm$ 1%. The deposits were about 200 μm thick. They were separated from the substrate in order to obtain free standing foils.

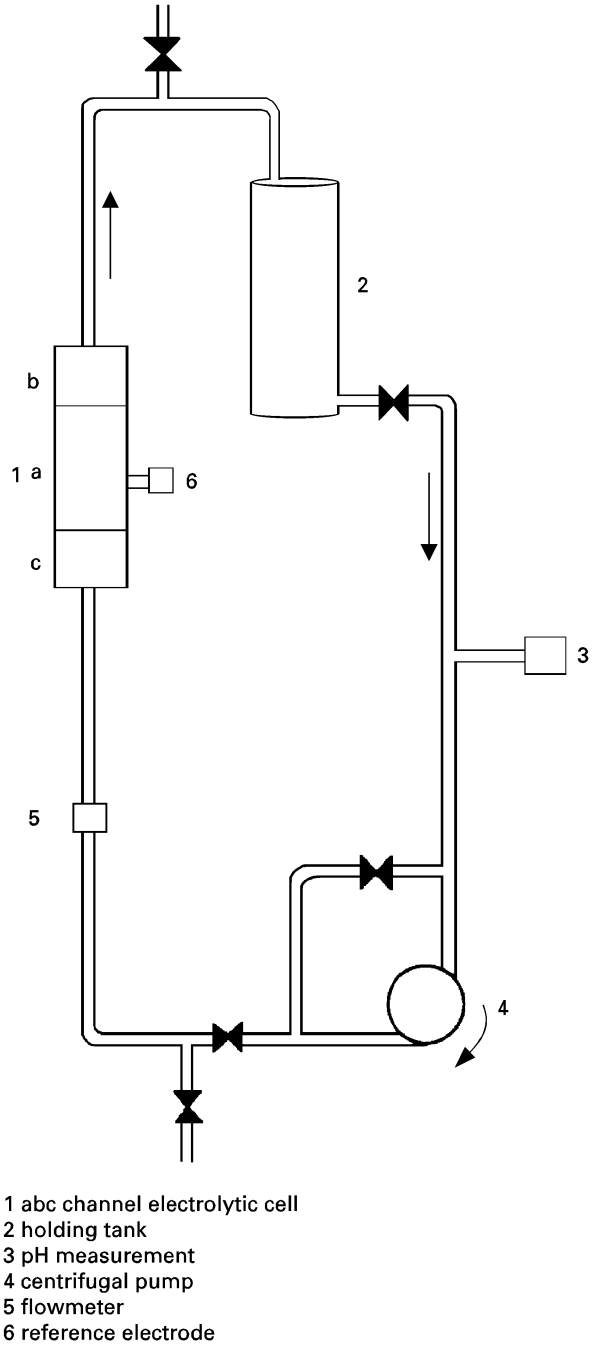

Figure 1 Schematic of the electrolytic cell where (1) is the abc channel electrolytic cell, (2) holding tank, (3) pH measurement, (4) centrifugal pump, (5) flowmeter and (6) reference electrode.

2.2. Microscopic characterization

The microstructures of the deposits were studied by optical microscopy, scanning electron microscopy (SEM) and transmission electron microscopy (TEM). The SEM observations were carried out using a Jeol JSM 820 scanning electron microscope which was used to examine the surface of the deposits and the fracture surfaces of tensile test specimens. Thin foil TEM analyses were carried out using a Philips CM20 ultratwin scanning transmission electron microscope. The thin foils were obtained by double jet electrolytic polishing with a solution of 10% perchloric acid in ethanol-2-butoxy at +5 °C (30 V).

2.3. X-ray diffraction analysis

The X-ray diffraction experiments were performed using a Siemens D 5000 diffractometer. Two methods were used to analyse the broadening of the diffraction peaks to enable the determination of crystallite size and lattice distorsions: the Warren–Averbach method [15] and the method of De Keijser *et al.* [16].

The powerful Warren–Averbach method is based on a rigorous analysis of "pure" peak profiles – corrected for the instrumental peak broadening – in terms of Fourier coefficients. This method requires two orders of reflection for each (*hkl*) plane considered and leads to an area-weighted crystallite size $\langle D \rangle_a$ and a mean square (local) strain $\langle e^2(L) \rangle$.

The method of De Keijser *et al.* is a rapid single line method for the determination of strain and crystal size by means of the use of a Voigt function to describe the peak profile shape function. A volume-weighted average crystallite size $\langle D \rangle_v$ is then defined as $\lambda/\beta_c^f \cdot \cos\theta$

and a strain value $\hat{e}$ as $\beta_g^f/4 \tan\theta$ where β_c^f and β_g^f are respectively the integral width of the Cauchy and the Gaussian components of the "pure" structurally broadened Voigt profile and λ and θ are respectively the X-ray $K\alpha_1$ wavelength and the angular position.

Averbach and Cohen [17] have developed a direct comparison method for the quantitative determination of the volume fractions of various phases in a randomly oriented multiphase polycrystalline aggregate. This method is based on the measurement of the integrated intensity of an isolated diffraction peak for each existing phase. Sage and Guillaud [18] applied this method to the quantitative determination of the proportion of α HCP and β FCC phases in cobalt powders. Using the most suitable α $(1\,0\,\bar{1}\,1)$ and β $(2\,0\,0)$ diffraction peaks they found the following relationship

$$\frac{x}{1-x} = k \cdot \frac{I_{\beta(200)}}{I_{\alpha(10\bar{1}1)}} \tag{2}$$

in which $I_{\beta(200)}$ and $I_{\alpha(10\bar{1}1)}$ are the measured integrated intensities, k is a constant depending on the radiation wavelength and x the volume fraction of the β FCC phase.

Preferred orientations, frequently observed in electrodeposits, introduce errors in the volume fraction determination. Thus it is necessary to replace the integrated intensity of one diffraction peak by the total intensity obtained from the corresponding complete pole figure [19]. Owing to the rotational symmetry in an electrodeposits texture, a plot of pole density versus angle ϕ between 0–90° gives a complete description of the texture; ϕ is the angle between the symmetry axis normal to the deposit surface and the normal towards the reflecting plane. The pole figure is then represented by the distribution curve of pole density I_ϕ versus angle ϕ. The calculation of total intensity from a pole figure should include the length of every parallel corresponding to I_ϕ. One obtains [20]:

$$I_{Tot} = 2\pi \int_0^{\pi/2} I_\phi \cdot \sin\phi \, d\phi \tag{3}$$

For the experimental determination of the pole density I_ϕ, it is necessary to use both a reflection and a transmission X-ray diffraction method.

The reflection method covers the inner part of the pole figure from $\phi = 0°$ to about 70° whereas the transmission method covers the outer part of the pole figure from ϕ values of about 50–90°. However, Scoyer *et al.* [19] have established with the help of crystallographic considerations that the data obtained by reflection are sufficient for the calculation of the total intensity from the pole figure for both α HCP and β FCC cobalt phases when rotational symmetry occurs.

In this work, the reflection method of Schulz [21] was used to obtain experimental α $(1\,0\,\bar{1}\,1)$ and β $(2\,0\,0)$ pole figures. Then, the corresponding total intensities were determined using Equation 3 and applying the arguments of Scoyer *et al.* [19]. Finally, these total intensities were introduced into Equation 2 in order to obtain the volume fraction of the β FCC phase.

2.4. Mechanical properties

Three testing methods were utilized to determine the mechanical properties of the deposits. Tensile tests were performed using an Instron machine. Samples were strained at 20 °C at a crosshead speed of 0.02 cm per min. Data were measured for the 0.2 per cent offset yield strength, ($R_{e0.2\%}$) ultimate tensile strength (R_m) and per cent elongation at fracture (A).

The ductility measurements were made by means of a work-hardening bend test. This test consists of applying cantilever bending to a strip piece clamped at one end; the specimen is bent backwards and forwards around two mandrels with a bend radius of 5 or 2 mm. This bending is repeated until fracture occurs. The bending ductility is defined as the number of cycles before fracture. In addition, Vickers micro hardness tests were performed with a 200 g load.

2.5. Hydrogen content determination

The hydrogen content of the electrodeposits were determined using a Leco RH 1 inert gas fusion apparatus.

3. Results and discussion

3.1. Electrochemical results

The influence of the pH of the solution on the current efficiency is shown in Fig. 2. The current efficiency, always greater than 85%, regularly increased as the pH increased and reached more than 99% at pH 3.5. This behaviour was due to hydrogen co-deposition at low pH and temperature.

Fig. 3 shows the cathodic potential as a function of the pH for deposits obtained at 50 °C. A sudden discontinuity is observed at a pH between 3.0–4.0. These results are in agreement with those reported for cobalt electrodeposition from chloride solutions [6].

3.2. Hydrogen content

The hydrogen contents shown in Fig. 4 were measured about 30 days after electrodeposition. The hydrogen content of the deposits increased when the pH or the electrolysis temperature decreased. It should be noted

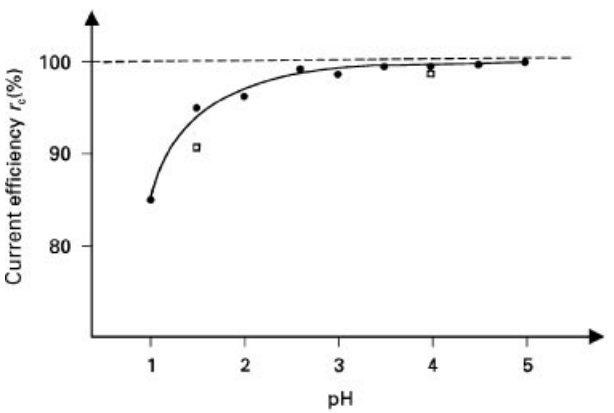

Figure 2 Current efficiency r_c versus pH (●) at 50 °C and (□) at 25 °C.

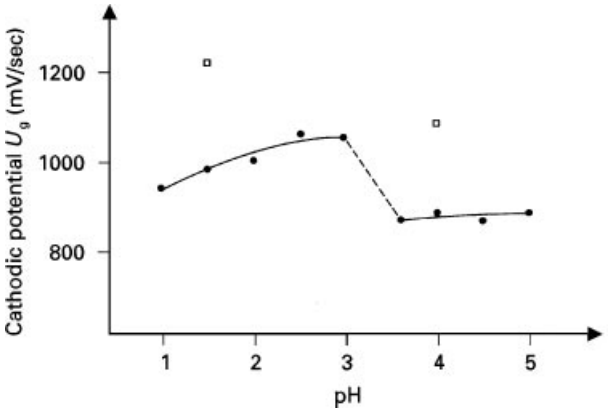

Figure 3 Cathodic potential U_g versus pH (●) at 50 °C and (□) at 25 °C.

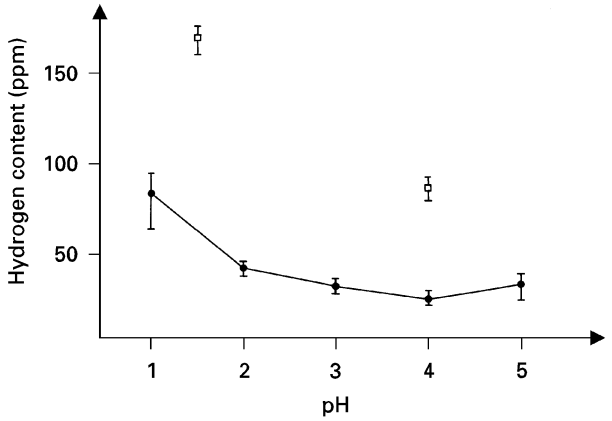

Figure 4 Hydrogen content measured 30 days after electrodeposition versus pH. (●) deposits obtained at 50 °C, (□) deposits obtained at 25 °C.

that for an individual deposit the hydrogen content did not change between 30 min and 100 days after the end of the electrodeposition.

The diffusion equations can be applied to the degassing phenomenon of a sheet of thickness h to enable the calculation of the average concentration $\bar{c}$ of hydrogen remaining inside the deposit at a time t after the end of the electrolysis.

The solution of the diffusion equation can be written as [22]

$$\bar{c}/c_0 = \frac{8}{\pi^2} \sum_{j=0}^{\infty} \frac{1}{(2j+1)^2} \exp\left(-\left[\frac{(2j+1)\pi}{\mathrm{h}} \right]^2 \cdot D \cdot t \right) \quad (4)$$

where c_0 = hydrogen concentration into the deposit at the end of the electrolysis

h = deposit thickness (200 μm, in our study)

D = diffusion coefficient of hydrogen in cobalt

From the data obtained by Caskey *et al.* [23], the diffusion coefficient of hydrogen in HCP cobalt. extrapolated to room temperature is $3.5 \times 10^{-12}\,\mathrm{cm^2\,s^{-1}}$. Using this value, Equation (4) gives

$\bar{c}/c_0 = 0.95$ for $t_1 = 30$ min and $\bar{c}/c_0 = 0.37$ for

$t_2 = 100$ days.

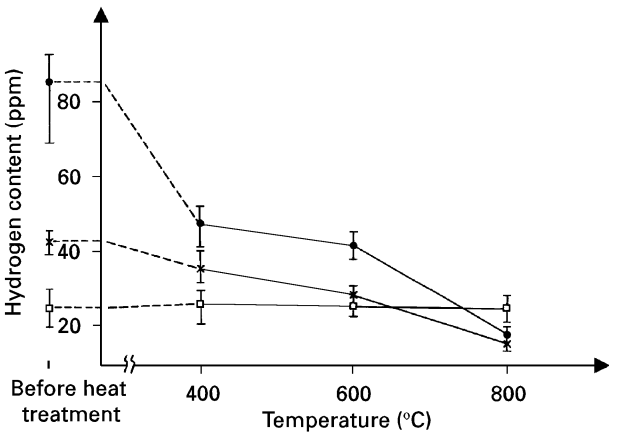

Figure 5 Hydrogen content measured after annealing for 1 h versus annealing temperature. (●) deposits obtained at pH 1, (×) deposits obtained at pH 2, (□) deposits obtained at pH 4.

Nevertheless as previously mentioned no change in hydrogen concentration was found in this study. This fact means that the detected hydrogen cannot diffuse out of the cobalt sheet at room temperature. To explain this, various possibilities have to be considered for the origin of this measured hydrogen: such possibilities include atomic or molecular hydrogen in microstructural trapping sites or an occluded chemical compound.

In order to investigate this question, annealing treatments were made on the cobalt deposits for 1 h at different temperatures. Fig. 5 shows the measured hydrogen contents in the deposits after annealing. For deposits obtained at pH 1 and pH 2, the hydrogen concentration decreased as the annealing temperature increased. This phenomenon can be explained most satisfactorily in terms of hydrogen detrapping during annealing. Hydrogen then escapes out of the deposit. No information is available in the literature on potential trap sites in the cobalt structure but they are probably the same as in iron or nickel where the main trapping sites have been determined to be dislocations and grain boundaries [24].

The larger hydrogen contents found in deposits obtained at pH 1 should be related to the more important hydrogen co-deposition observed at this pH value. On the other hand, the measured hydrogen content for deposits obtained at pH 4 remained unchanged with increasing annealing temperature. In this case the detected hydrogen probably comes from the decomposition of some occluded cobalt compound such as $Co(OH)_2$. The occlusion of this compound during cobalt electrodeposition at high pH values has already been mentioned in the literature [6].

3.3. X-ray diffraction patterns

The X-ray diffraction patterns measured on the deposits obtained at 50 °C, at pH 1 to 3, revealed no significant preferred orientation (Fig. 6a) but, a too weak α (0 0 0 2) peak intensity was noticed; [α (0 0 0 2) + β (1 1 1), if both phases coexist]. For the deposit obtained at pH 1, a weak β (2 0 0) extra reflection was detected.

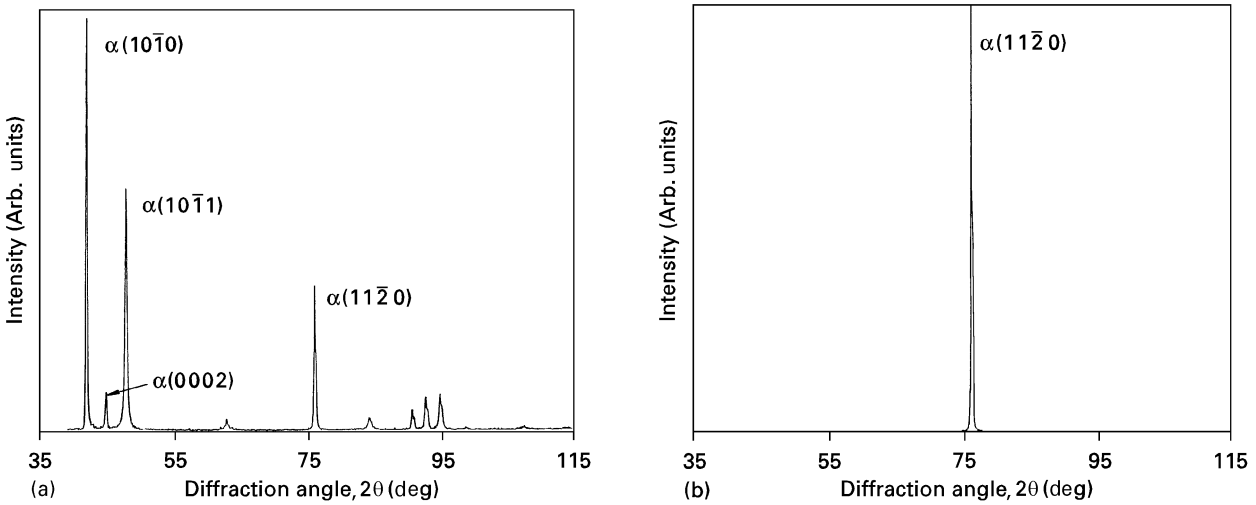

Figure 6 X-ray diffraction patterns, (a) from a deposit obtained at pH 1.5 and T = 50 °C; (b) from a deposit obtained at pH 4 and T = 50 °C.

TABLE I β(FCC) phase volume fraction x in the deposits

Electrolysis conditions	x
pH 5; 50 °C	≤ 1%
pH 4.5; 50 °C	≤ 1%
pH 4; 50 °C	≤ 1%
pH 3.5; 50 °C	= 1.5%
pH 3; 50 °C	= 1.5%
pH 2; 50 °C	= 5.5%
pH 1.5; 50 °C	= 7%
pH 1; 50 °C	= 12%
pH = 4; 25 °C	= 14.5%
pH = 1.5; 25 °C	= 22%

For the deposits obtained at 25 °C (pH 1.5 and 4) and at 50 °C (pH > 3), only one peak [α (1 1 $\bar{2}$ 0) or, if both phases coexist, α (1 1 $\bar{2}$ 0) + β (2 2 0)] was observed (Fig. 6b). Such deposits are perfectly textured.

3.4. Determination of the volume fractions of the α (HCP) and β (FCC) phases

Table I summarizes the β (FCC) phase volume fractions in the deposits. These volume fractions were determined by means of the above described procedure using pole figures obtained by the reflection method of Schulz.

Comparing Table I to Fig. 4, it is apparent that the β (FCC) content depends on the hydrogen concentration in the deposit. A larger concentration of incorporated hydrogen leads to a larger β (FCC) volume fraction. This observation confirms the dominant influence of incorporated hydrogen on β face centered cubic phase formation as proposed by various authors [6, 7, 25].

It should also be noted that the β (FCC) modification can exist in the two different types of deposits nearly random oriented or strongly textured.

Finally, the pole figures definitely confirm the observations from the measured X-ray diffraction patterns.

3.5. X-ray diffraction line profile analysis

Tables II and III respectively list the average crystallite sizes $\langle D \rangle_v$ and the strain values $\hat{e}$ obtained by the method of De Keijser *et al.* [16] from different α (HCP) diffraction peaks for the non-significantly textured deposits. Table IV contains $\langle D \rangle_v$ and $\hat{e}$ calculated in the same way from the single α (1 1 $\bar{2}$ 0) line profile for the almost perfectly (1 1 $\bar{2}$ 0) textured deposits.

Table V summarizes the results obtained by the Warren–Averbach method. This method cannot be applied to perfectly textured deposits because the second order α (2 2 $\bar{4}$ 0) peak is not available. From these results, three main considerations have to be made.

(i) First, the $\langle D \rangle_v$ values calculated from ($h\,k\,i\,l$) diffraction peaks with $h - k = 3n \pm 1$ and $l \neq 0$ [e.g.,

TABLE II Average crystallite sizes $\langle D \rangle_v$ (in nm) obtained by the method of De Keijser *et al.* [16] from various α(HCP) diffraction peaks for the non-significantly textured deposits

Diffraction peak	pH 1	pH 1.5	pH 2	pH 3
(1 0 $\bar{1}$ 0)	53.2	151.8	241.3	181.0
(1 0 $\bar{1}$ 1)	11.7	18.5	33.7	45.3
(1 1 $\bar{2}$ 0)	40.8	101.3	172.7	103.2
(1 0 $\bar{1}$ 3)	8.0	14.5	28.9	39.5
(2 0 $\bar{2}$ 0)	51.4	90.7	142.0	120.7
(2 0 $\bar{2}$ 1)	20.1	27.6	65.7	61.1

TABLE III Strain values $\hat{e}$ obtained by the method of De Keijser *et al.* [16] from various α(HCP) diffraction peaks for the non-significantly textured deposits

Diffraction peak	pH 1	pH 1.5	pH 2	pH 3
(1 0 $\bar{1}$ 0)	0.0017	0.0008	0.0006	0.0008
(1 0 $\bar{1}$ 1)	0.0014	0.0012	0.0009	0
(1 1 $\bar{2}$ 0)	0.0019	0.0011	0.0005	0.0009
(1 0 $\bar{1}$ 3)	0.0006	0.0007	0.0003	0
(2 0 $\bar{2}$ 0)	0.0011	0.0008	0.0006	0.0006
(2 0 $\bar{2}$ 1)	0.0022	0.0009	0.0011	0.001

TABLE IV $\langle D \rangle_v$ and $\hat{e}$ obtained by the method of De Keijser *et al.* [16] for the single $\alpha\ (1\,1\,\bar{2}\,0)$ line profile for the almost perfectly $\alpha\ (1\,1\,\bar{2}\,0)$ textured deposits

Electrolysis conditions	$\langle D \rangle_v$ (μm)	$\hat{e}$
pH 5; 50 °C	> 1	0.0004
pH 4,5; 50 °C	> 1	0
pH 4; 50 °C	> 1	0.0004
pH 3.5; 50 °C	> 1	0
pH 4; 25 °C	0.3982	0.001
pH 1.5; 25 °C	0.0733	0.0053

TABLE V Results of the Warren–Averbach [15] line profile analysis

Electrolysis conditions	$\langle D \rangle_a$ (nm)	$\langle e^2(L) \rangle^{1/2}$ L = 5.0 nm
pH 1; 50 °C	31.0	0.00338
pH 1,5; 50 °C	83.0	0.00293
pH 2; 50 °C	104.0	0.00148
pH 3; 50 °C	72.0	0.00227

$\alpha\ (1\,0\,\bar{1}\,0)$] are smaller than those obtained from the other peaks [e.g., $\alpha(1\,0\,\bar{1}\,1|)$].

This behaviour could be due to the existence of stacking faults in the electrodeposits. Indeed the general theory of X-ray diffraction from faulted HCP structures indicates a broadening due to stacking faults for diffraction lines with $h - k = 3n \pm 1$ and $1 \neq 0$. This line broadening does not affect the strain values but leads to a calculated "effective" size smaller than the true crystallite size. The occurrence of numerous stacking faults in the deposits is confirmed by the microscopy investigations that will be described in the following section.

(ii) Comparing the calculated microstrain values to hydrogen contents shown on Fig. 4, it seems that the hydrogen co-deposition results in the formation of crystalline defects that are the cause of the obtained microstrains.

(iii) Both the Warren–Averbach method and the De Keijser *et al.* method indicate that the crystallite size for electrodeposits obtained at pH 1 and T = 50 °C is significantly smaller than for electrodeposits obtained at other experimental conditions. This is also confirmed by microscopy observations and suggests that, during the electrodeposition at pH 1 (50 °C), the nucleation rate is higher.

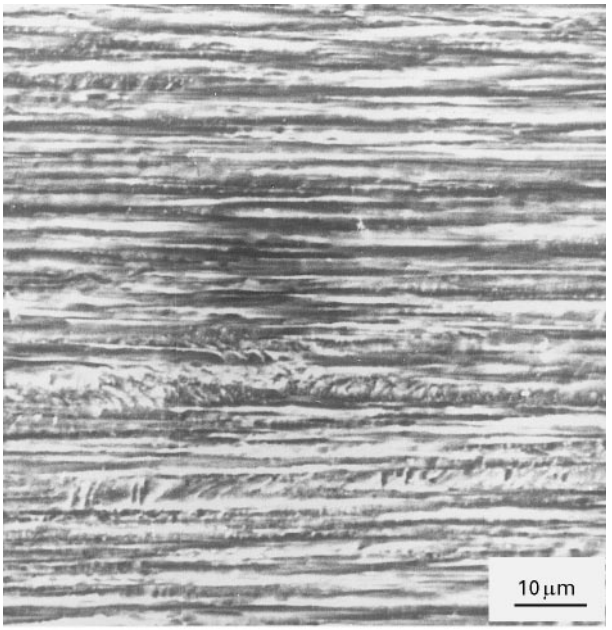

Figure 7 Cross-sectional SEM image of a cobalt electrodeposit obtained at pH 5 and T = 50 °C. Deposit growth direction: from left to right.

Figure 8 TEM micrograph of a deposit obtained at pH 5 and T = 50 °C. Section parallel to the substrate.

3.6. Microscopy investigations

Two different characteristic structures were observed in the deposits. These structures are in fact those most commonly encountered in cobalt electrodeposits. Each structure is exactly related to one type of deposit determined by the X-ray diffraction analysis namely an almost perfectly textured deposit or a nearly random oriented deposit.

The first structure was found in all strongly textured deposits (50 °C, pH > 3; 25 °C, pH 1.5 and 4). It corresponds to a F T (field oriented texture) type in Fisher's classification [26]. The columnar aspect of this structure is revealed in Fig. 7 which shows an SEM cross-sectional picture. This cross-section had previously been polished and etched.

Fig. 8 is a TEM micrograph of a thin foil parallel to the substrate for a deposit obtained under the same conditions as those for Fig. 7. For such a section the grain structure is equiaxed.

Figure 9 Electron diffraction pattern from crystal 1 on Fig. 8, zone axis [0 1 $\bar{1}$ 0] (spots (0 0 0 *n*), *n* odd, are double diffraction spots).

All the grains have electron diffraction patterns similar to the one represented by Fig. 9. Its zone axis is [0 1 $\bar{1}$ 0]. This fact confirms the strong α (1 1 $\bar{2}$ 0) texture. The electron diffraction patterns also reveal that in many cases two adjacent grains are slightly misoriented (3° for example between grain 3 and grain 4 in Fig. 8) around the zone axis. In other cases, the misorientation is greater (15° between grain 1 and grain 2). The closely spaced parallel lines observed in each grain represent the intersection of the basal plane

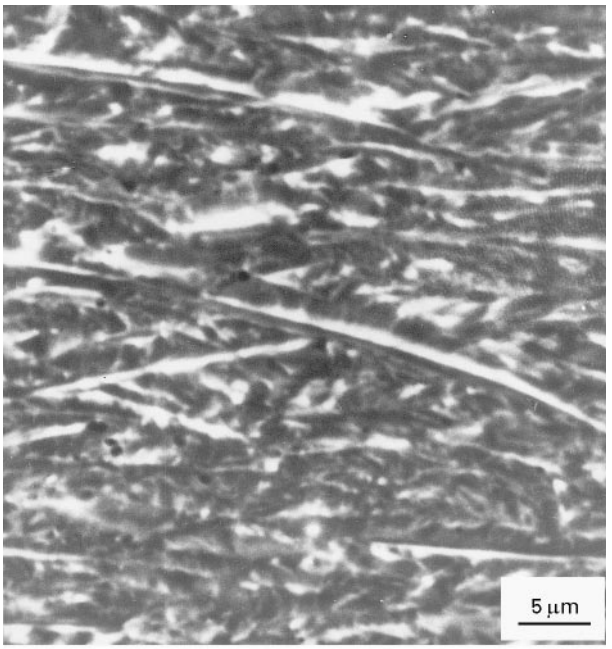

Figure 10 Cross-sectional SEM image of a cobalt electrodeposit obtained at pH 2 and T = 50 °C. Deposit growth direction: from left to right.

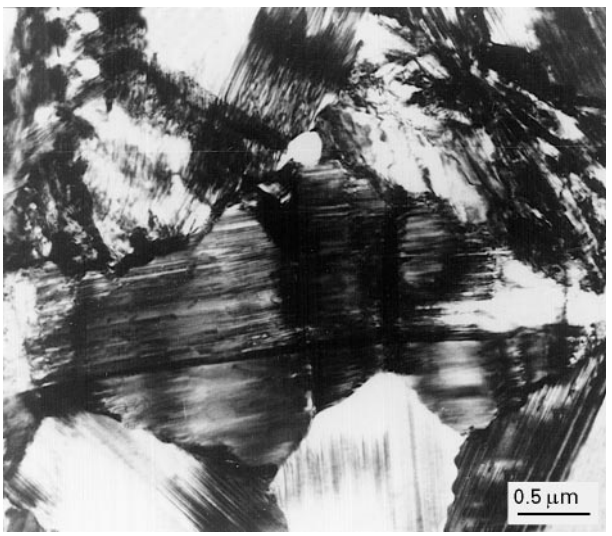

Figure 11 TEM micrograph from a deposit obtained at pH 1.5 and T = 50 °C. Section parallel to the substrate.

(0 0 0 2) with the plane of the foil and are due to stacking faults.

Nearly random oriented cobalt deposits (50 °C, pH 1 to 3) exhibit a totally different structure. Their structure consists of an assembly of dihedrons. A SEM cross-sectional image (Fig. 10) reveals three dimensional nucleation. Figs. 11 and 12 are TEM micrographs of thin foils parallel to the substrate. These figures show the dihedral shape of the crystallites. The curvature of the ridge between part A and part B for the dihedron seen in Fig. 12 results from the fact that each part of the dihedron is not a single crystal but consists of a series of subgrains. The electron diffraction patterns indicate a weak misorientation between two adjoining subgrains (about 2°). The electron diffraction analysis (Fig. 13) moreover reveals that both parts of a dihedron have a twin relationship to one

another. The twin plane (TT) lies perpendicular to the substrate and contains the ridge of the dihedron.

The observed structure in nearly random oriented cobalt electrodeposits is identical to the "pseudo random" structure mentioned by Sard *et al.* [1] Similar dihedral shapes have been reported in (2 1 1) textured FCC nickel electrodeposits by various authors [27, 28].

Thevenin [29] and Atanassov *et al.* [30] have proposed that the (2 1 1) texture in nickel electrodeposits is initiated by the development of paracrystalline decahedral and icosahedral clusters. The authors of this paper think that a further elucidation of the crystalline structures forming in cobalt electrodeposits, which is beyond the scope of this study should take into account the similarity with nickel electrodeposits.

A characteristic surface morphology corresponds to each type of deposit microstructure. Almost perfectly textured $\alpha(1\,1\,\bar{2}\,0)$ cobalt electrodeposits exhibit a smooth surface (Fig. 14) with a satin like appearance while nearly random oriented deposits exhibit curved dihedral shapes on their surfaces (Fig. 15) with a dull dark grey or black appearance. The surface morphology shown in Fig. 15 is commonly mentioned in the investigations of cobalt electrodeposits [1, 6, 31].

3.7. Mechanical properties of the deposits

Conventional Vickers microhardness tests do not reveal significant differences between the electrodeposits obtained at 50 °C (Fig. 16). On the other hand, the microhardness of the electrodeposits obtained at 25 °C is clearly higher. This fact can be explained by the higher microstrain values, $\hat{e}$, for these deposits.

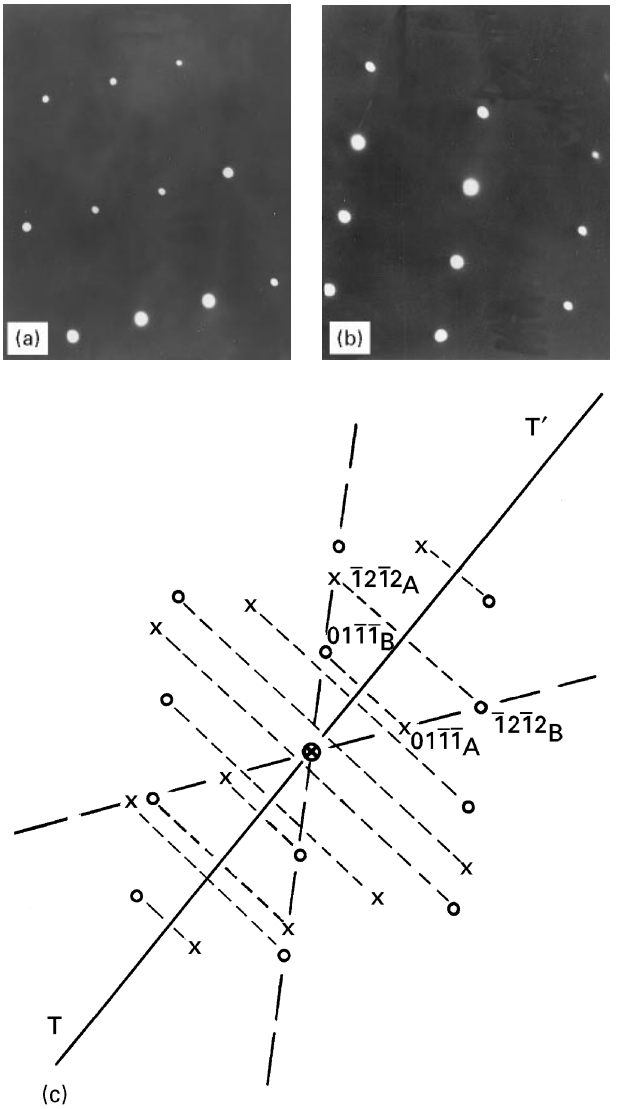

Figure 13 (a) Electron diffraction pattern of crystal A (on Fig. 12), (b) electron diffraction pattern of crystal B (on Fig. 12), (c) crystallographic relationship between (×) crystal A and (○) crystal B.

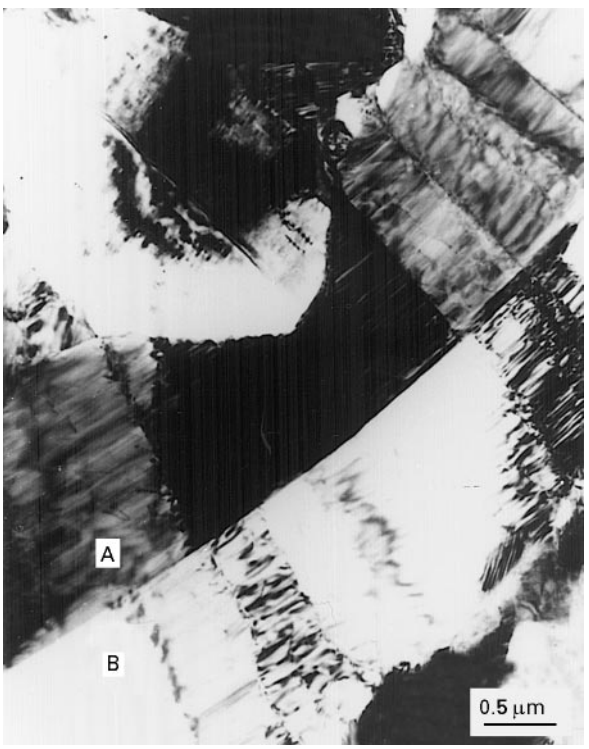

Figure 12 TEM micrograph of a deposit obtained at pH 2 and T = 50 °C. Section parallel to the substrate.

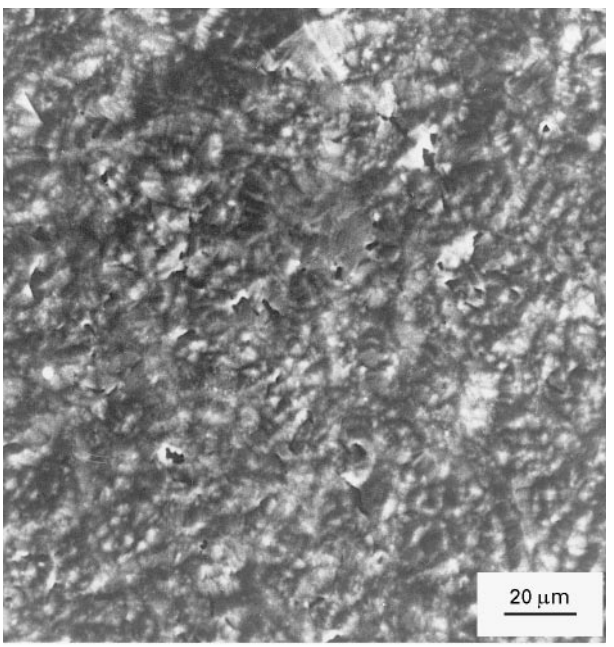

Figure 14 SEM image of the surface of a deposit obtained at pH 4 and T = 50 °C.

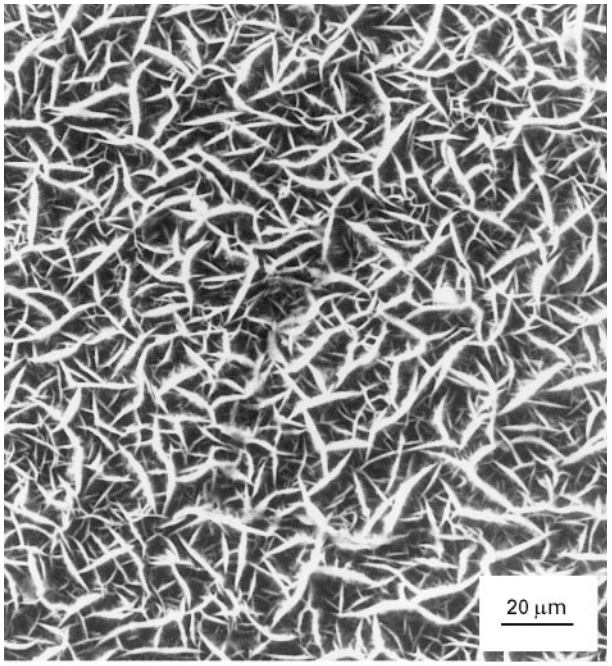

Figure 15 SEM image of the surface of a deposit obtained at pH 1.5 and T = 50 °C.

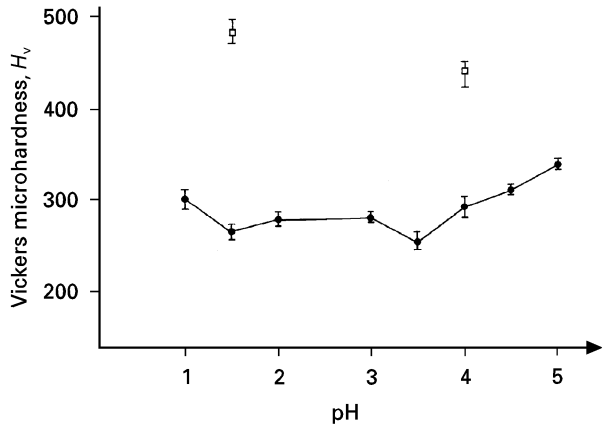

Figure 16 Vickers microhardness versus pH. (●) deposits obtained at 50 °C, (□) deposits obtained at 25 °C.

TABLE VI Summary of tensile test results (deposits obtained at $T = 50$ °C)

Electrolysis conditions	A (%)	$R_{e;0.2\%}$ (MPa)	R_m (MPa)
pH 5	0.5	430	455
pH 4	0.8	435	480
pH 3	5.9	335	565
pH 2	5.1	315	540
pH 1.5	2.8	385	550
pH 1	2.1	450	620

TABLE VII Summary of work-hardening bend test results (deposits obtained at $T = 50$ °C)

Electrolysis conditions	Number of bends before fracture	
	bend radius 5 mm	bend radius = 2 mm
pH 5	0	0
pH 4	0	0
pH 3	53	23
pH 2	28	15
pH 1.5	26	6
pH 1	13	2

The mechanical properties measured by tensile test are much more sensitive to microstructure than microhardness as is shown in Table VI. For the nearly random oriented cobalt electrodeposits, the ductility decreases when the pH value of the electrolyte decreases.

Consequently, the higher β (FCC) phase content produced in deposits at low pH does not correspond to an increase of ductility as was expected. This is probably due to the presence of trapped hydrogen in this kind of deposit; severe embrittlement can indeed be produced in FCC and HCP metals by very small amounts of hydrogen [32]. It should also be noted that the smaller grain size for deposits obtained at pH 1 leads to a higher yield strength and tensile strength.

The reason for the total lack of ductility in strongly textured electrodeposits is not fully understood. Nevertheless, an annealing treatment at 400 °C for

TABLE VIII Summary of main observations

Type of deposits	1a	1b	2
Electrolysis conditions	$T = 50$°C; pH > 3	$T = 25$°C; pH 1.5 or 4	$T = 50$ °C; p ≤ 3
structure	columnar structure	columnar structure	assembly of dihedrons
texture	very strong $\alpha(11\bar{2}0)$ texture	very strong $\alpha(11\bar{2}0)$ + β(220) texture	nearly random oriented
hydrogen content	low	high	varying; increases if pH decreases
β(FCC) phase content	nil	rather high (up to 22%)	varying; increases if pH decreases
ductility	very weak	extremely weak	rather weak: varying; decreases if pH decreases
surface	satin like or grey pale; relatively smooth	satin like or grey pale; relatively smooth	dull dark grey or black; rather rough

these deposits indicates that their prismatic grain morphology and pronounced preferred crystallographic orientation are not the main structural features limiting the ductility. Indeed, after a 1 h annealing at 400 °C the elongation A for a cobalt deposit at pH 4 or pH 5 increases from less than 1% up to about 8% while the grain morphology and the strong texture remain. Furthermore, this result shows that it would be very interesting to systematically study the effect of annealing in order to maximize the ductility of cobalt electrodeposited foils.

Owing to their brittleness, no tensile test specimen could be made from deposits obtained at 25 °C. This brittleness was probably due to both the structure and the high hydrogen content of such deposits.

The work-hardening bend tests confirm the tensile test results. They allow the distinction between the non ductile strongly textured and the nearly random oriented types of deposits to be made (see Table VII).

4. Conclusions

The main observations of this investigation are listed in Table VIII. Depending on the electrolysis parameters, two types of cobalt electrodeposits were obtained in chloride solutions. Their structures were completely different in that:

(1) the first type of deposit was a FT (field oriented texture) type. Its columnar structure consisted of narrow prismatic crystallites with a strong αHCP $(1\,1\,\bar{2}\,0)$ [βFCC (220)] preferred orientation; the surface of these satin like or pale grey deposits was relatively smooth, this type of deposit was obtained under the following electrolysis conditions: $T = 50\,^{\circ}C$, pH > 3; $T = 25\,^{\circ}C$, pH 1.5 or 4.

(2) the second type of deposit consists of an assembly of dihedrons with nearly random crystallographic orientation; the surface of these dull dark grey or black deposits was rather rough. This type of deposit was obtained under the following electrolysis conditions: $T = 50\,^{\circ}C$, pH ≤ 3.

A sudden discontinuity in the cathodic potential appeared exactly at the transition between these two different structures.

The ductility of each kind of deposit was significantly different. The F.T. type of deposit had no ductility compared to the nearly random oriented cobalt electrodeposits. On the other hand, the higher β(FCC) phase content in deposits obtained al low pH values did not correspond to an increase of ductility as expected. This seems to be due to the trapped hydrogen that always exists in these deposits.

On the other hand, an annealing treatment clearly improves the ductility of the cobalt electrodeposits. This seems to be the most promising means to optimize the malleability of cobalt foils obtained by electrodeposition. Therefore, the effects of an annealing treatment on the structure and mechanical properties of cobalt electrodeposits will be studied in a further publication.

References

1. R. SARD, C. D. SCWARTZ and R. WEIL, *J. Electrochem. Soc.* **113** (1966) 424.
2. M. FROMENT and G. MAURIN, *C.R. Acad Sc. Paris-Série C* **266** (1968) 1017.
3. C. FENEAU and R. BRECKPOT, *A.T.B. Métallurgie* **9** (1969) 115.
4. S. VITKOVA, S. ARMIANOV and N. PANGAROV, *Electrodepos. Surf. Treat.* **3** (1975) 225.
5. J. SCOYER and R. WINAND, *Surf. Techn.* **5** (1977) 169.
6. S. NAKAHARA and S. MAHAJAN, *J. Electrochem. Soc.* **127** (1980) 283.
7. I. POVETKIN and I. KOVENSKII, *Sov. Electrochem.* **22** (1986) 1101.
8. M. F. QUINN and I. M. CROLL, *Adv. X-Ray Anal* **4** (1961) 151.
9. R. D. FISHER, *J. Electrochem. Soc.* **109** (1962) 479.
10. S. ARMYANOV and S. VITKOVA, *Surf. Techn.* **7** (1978) 319.
11. J. DILLE, PhD thesis, Université Libre de Bruxelles (1994).
12. R. W. FRASER, D. J. L. EVANS and V. N. MACKIW, *Cobalt* **25** (1964) 171.
13. M. BECKERS, L. FONTAINAS, B. TOUGARINOFF and L. HABRAKEN, *ibid* **25** (1964) 171.
14. E. DIDERICH, J. M. DRAPIER, D. COUTSOURADIS and L. HABRAKEN, *Le Cobalt* **1** (1975) 7.
15. B. E. WARREN and B. L. AVERBACH, *J. Appl. Phys.* **23** (1952) 497.
16. Th. H. DE KEIJSER, J. L. LANGFORD, E. J. MITTEMEIER and A. B. P. VOGELS, *J. Appl. Cryst.* **15** (1982) 308.
17. B. L. AVERBACH and M. COHEN, *Trans. Met. Soc. AIME* **176** (1948) 104.
18. M. SAGE and CH. GUILLAUD, *Rev. Met.* **47** (1950) 139.
19. J. SCOYER, R. WINAND and J. CHARLIER, *ATB Métallurgie* **15** (1975) 222.
20. B. D. CULLITY, "Elements of X-Ray diffraction", 2nd Edn (Addison-Wesley, Reading, MA, 1978).
21. L. G. SCHULTZ, *J. Appl. Phys.* **20** (1949) 1030.
22. P. SHEWMON, "Diffusion in solids", 2nd Edn (The Minerals Metals and Materials Society, Warrendale, PA 1989).
23. G. R. CASKEY, R. G. DERRICK and M. R. LOUTHAN, *Scipta Metall.* **8** (1974) 481.
24. SUNG MAN LEE and JAI YOUNG LEE, *Met. Trans. A* **17** (1986) 181.
25. G. MAURIN, Thesis, Faculté des Sciences de Paris (1970).
26. H. FISCHER, "Electrolytische Abscheidung und Elektrokristallisation von Metallen" (Springer Verlag, Berlin, 1954).
27. H. SCHLÖTTERER, *Z. Kristall* **119** (1964) 321.
28. M. FROMENT and G. MAURIN, *J. Microsc. Spectrosc. Electron* **12** (1987) 379.
29. J. THEVENIN, *ibid* **1** (1976) 7.
30. N. ATANASSOV, S. VITKOVA and S. RASHKOV, *Surf. Technol* **14** (1981) 215.
31. M. ROJAS, C. L. FAN, H. J. MIAO and D. L. PIRON, *J. Appl. Electroch.* **22** (1992) 1135.
32. G. DIETER, "Mechanical Metallurgy" (3rd Edn) (McGraw Hill, New York, 1986).

Received 25 March
and accepted 2 July 1996